FAILURE STRENGTH PREDICTION FOR CFRP-STIFFENED PANEL

Go Matsubara*, Fumihide Inamura*, Hirokazu Matsuda*
*** Kawasaki Heavy Industries, Ltd.**

Keywords: *postbuckling, fracture toughness, energy release rate, stiffened panel, compression load, shear load, debonding, CFRP*

Abstract

The fracture mechanics approach for predicting the failure strength after buckling in a composite stiffened panel was proposed. The failure after buckling was caused by the debonding between the skin and the stiffener. Therefore, the stiffened panel was postbuckling-analyzed by the finite element method to compute the element force at the end of the stiffener flange. The skin-stiffener strip model that had a virtual crack was used to compute the energy release rates (G-values) per unit load. The G-values at the end of the stiffener flange were calculated by combining the element forces and the G-values per unit load. The proposed method was to calculate the failure strength on the basis of the failure criterion that was obtained from the fracture toughness tests, for the debonding between the skin and the stiffener. The failure loads of the compression and shear buckling tests in reference [3] were predicted. This method showed a good correlation between predicted failure load and measured failure load.

1 Introduction

Composite stiffened panels are widely used in aircraft, including Boeing 787. To reduce the weight of composite stiffened panels in fuselages, it is necessary to use a postbuckling design. Composite stiffened panels have skin/stiffener configurations. Therefore, failure after buckling is caused by the debonding between the skin and the stiffener, as shown in Figure 1. Recent studies [1, 2] have focused on this debonding and have suggested the method of predicting the debonding strength on the basis of fracture mechanics. However, the emphasis of those studies was on the method of computing the energy release rate G, and no practical method of calculating the failure strength of stiffened panels was described.

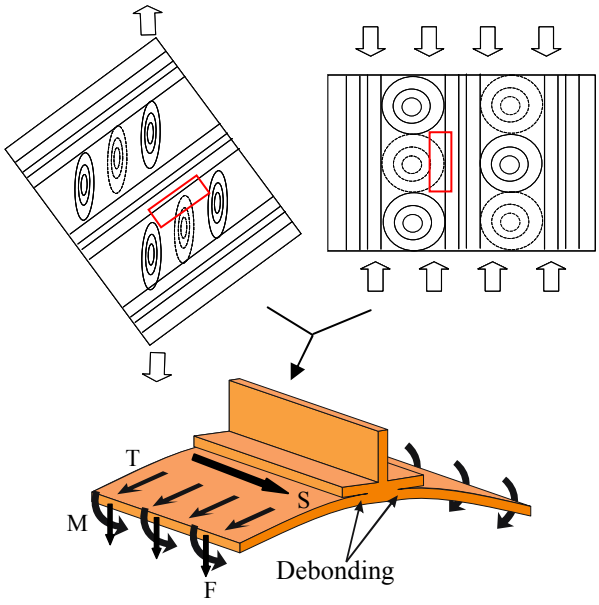

Fig. 1. Debonding between skin and stiffener.

The objective of this study is to develop the method of predicting the failure strength of composite stiffened panels after buckling. The failure loads of the compression and shear buckling tests in reference [3] are predicted. The predicted values are compared with the test results [3].

2 Approach to failure strength prediction

The sequence of the proposed method of predicting the failure strength is described below.

(1) Computing the element force at the end of the stiffener flange in the stiffened panel model (postbuckling analysis).

(2) Computing the G_0-values per unit load in the skin-stiffener strip model (G-value analysis).

(3) Calculating the G-values at the end of the stiffener flange by combining the element forces and the G_0-value per unit load (G-value superposition).

(4) Predicting the failure load on the basis of the failure criterion that was set for the fiber direction angle of the skin/stiffener interface.

The features of this method are as follows:

(1) The failure strength for an undamaged stiffened panel that has no flaw can be predicted.

(2) When the loading condition varies, recomputing the G_0-values per unit load by the finite element method (FEM) is not necessary because FEM analysis has two parts.

(3) The failure criterion is set for each fiber direction angle of the delamination interface. Therefore, the accuracy of the failure strength prediction is improved.

3 Results and discussion

3.1 Fracture toughness test

To establish the failure criterion for the debonding between the skin and the stiffener, fracture toughness tests were carried out with the double cantilever beam (DCB) for mode I, the end-notched flexure (ENF) for mode II, the mixed mode bending (MMB) for the mixed mode, and the edge crack torsion (ECT) specimens for mode III. The tested material was Toho Tenax UT500/#135, which was the one used for the stiffened panels in reference [3]. The mechanical properties of the material are summarized in Table 1. The stacking sequence of test specimens is given in Table 2. The stacking sequence was classified into two cases. Specimen-A, B and C have the same delamination angle of 0//0 but different elastic modulus in the longitudinal direction of the specimen. Specimen-D and E have different delamination angles but the

Table 1. Mechanical properties of materials [3].

Material		Toho Tenax QU135-197A
fiber		UT500
Epoxy resin		131
Elastic constants	E_1 (GPa)	131
	E_2 (GPa)	8.61
	G_{12} (GPa)	4.19
	ν_{12}	0.29
Ply thickness	t (mm)	0.189

Table 2. Stacking sequence of test specimens.

Specimen Type	Specimen No.	Stacking sequence	Delamination interface angle
DCB ENF MMB	A	$0_8//0_8$	0//0
	B	$0/(0/90)_3/0//0/(90/0)_3/0$	
	C	$(\pm45/90/0)_2//(0/90/\mp45)_2$	
	D	$(0/90/\pm45)_2//\pm45/90/0/\mp45/90/0$	+45//-45
	E	$(\pm45/90/0)_2//90/0/\mp45/0/90/\mp45$	0//90
ECT	F	$(0/90/\pm45)_S//(0/90/\pm45)_S$	0//0
	G	$(\pm45/0/90)_S//\mp45/90/0/0/90/\mp45$	+45//-45

// : the position of the starter delamination

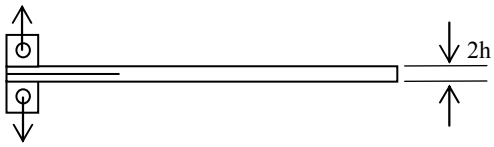

(a) Double cantilever beam

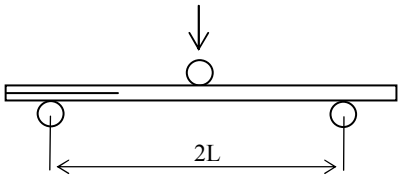

(b) End-notched flexure

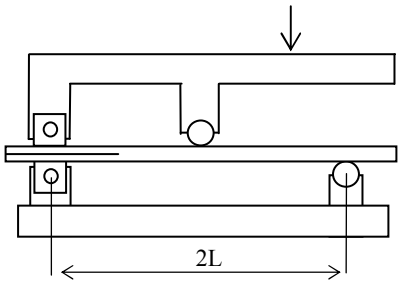

(c) Mixed mode bending

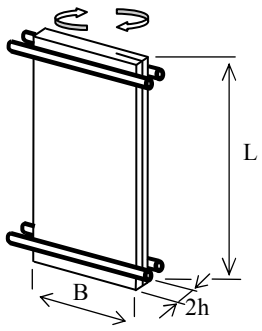

(d) Edge crack torsion

Fig. 2. Fracture toughness test specimens.

same modulus in the longitudinal direction of the specimen. The configurations of the test specimen are shown in Fig. 2. The specimen size was the same among the DCB, the ENF and the MMB specimens. The width B was 20 mm and the thickness 2h was 3.02 mm. The span 2L was 100 mm in both the ENF and MMB tests. The width B was 40 mm, the length L was 80 mm and the thickness 2h was 3.02 mm in the ECT specimen. The fracture toughness was calculated by the compliance method in all specimens.

The averages of the fracture toughness for each mode are given in Table 3. Figure 3 shows the results of the DCB, ENF and MMB tests. The broken line in the figure represents equation (1) in which each average of G_{IC} and G_{IIC} was substituted at a delamination interface of 0//0. The solid line in the figure represents equation (1) in which each average of G_{IC} and G_{IIC} was substituted at delamination interfaces of 0//90 and +45//-45. The exponent n of equation (1) was set to 1.5 in both cases. Equation (1) and fracture toughness test results agreed well. The failure criterion is defined by equation (1). Figure 4 shows the failure criterion. The area outside this region is the fracture region.

$$(G_I/G_{IC})^n+(G_{II}/G_{IIC})^n+(G_{III}/G_{IIIC})^n=1 \qquad (1)$$

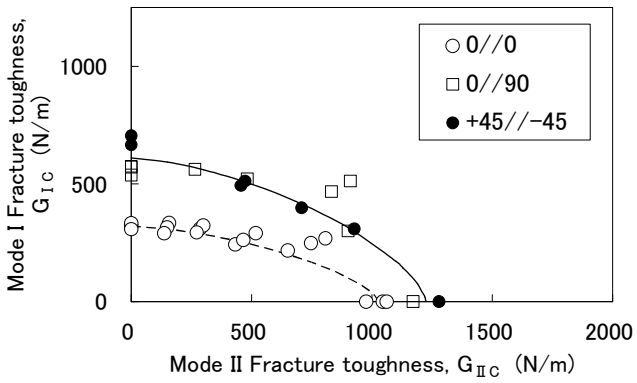

Fig. 3. Mixed mode fracture toughness.

Table 3. Fracture toughness of G_{IC}, G_{IIC} and G_{IIIC}.

unit : J/m^2

Delamination interface angle	G_{IC}	G_{IIC}	G_{IIIC}
0//0	321	1028	1714
+45//-45	611	1225	877
0//90			-

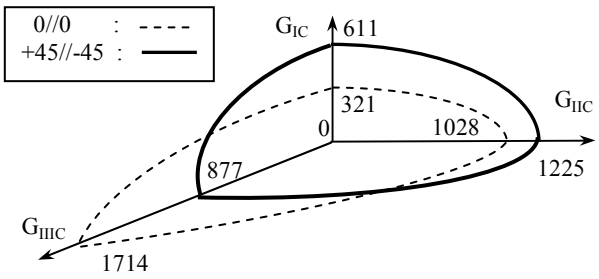

Fig. 4. Failure criterion of skin/stiffener interfaces.

3.2 Method of calculating energy release rate

First, the procedure for computing the G_0-values per unit load at the end of the stiffener flange is proposed. Next, the method of calculating the G_I, G_{II} and G_{III} at the end of the stiffener flange is explained by combining the G_0-values per unit load and the element forces.

The G_0-values per unit load at the end of the stiffener flange were computed with shell elements by Wang's method [1]. Figure 5 shows the details of the FEM shell model for computing G_0-values. The skin nodes and stiffener flange nodes are offset from the midplane of shell elements to the interface between the skin and the stiffener flange. The corresponding skin and stiffener flange nodes have identical translation and rotational degrees of freedom.

Figure 6 shows the skin-stiffener strip shell model for computing the G_0-values per unit load at the end of the stiffener flange. This model is perpendicular to the edge of the stiffener flange. A crack is assumed at the interface between the skin and the stiffener flange. Wang computed the G-values for bending moment M and out-of-plane shear load F. In the proposed method, the G-values for tension load T and in-plane shear load S were also computed. The stiffener center of the skin-stiffener strip shell model is clamped. Both sides of the FEM model for tension load T, bending moment M and out-of-plane shear load F have symmetric boundary conditions. The boundary conditions were changed for in-plane shear loading S. Both sides of the FEM model for in-plane shear load S have periodic boundary conditions. The width of the FEM model is one element. The applied loads T, F and S are all unit loads of 1 N/mm. The applied moment M is 1 Nmm/mm.

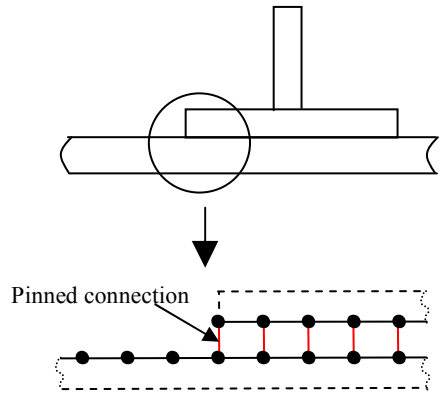

Fig. 5. FEM shell model for G-value analysis.

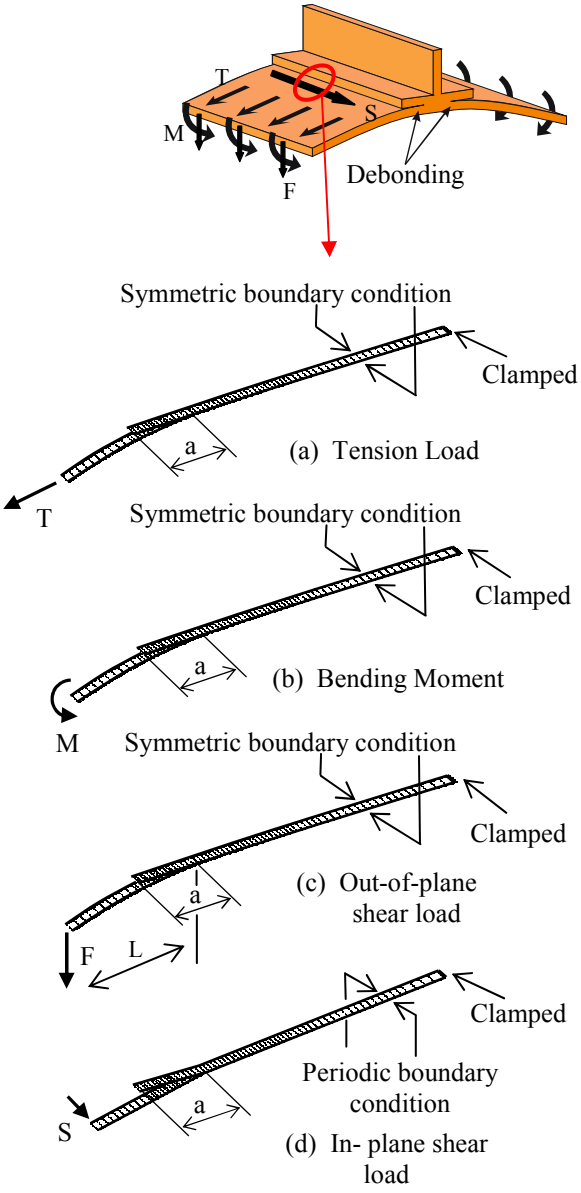

Fig. 6. Skin-stiffener strip shell model.

For each loading condition, the G-values were verified to be constant for various crack lengths. The crack length of the FEM model is set as 5 mm from the analysis results.

When the shear or compression load is applied to the stiffened panel, the G_I, G_{II} and G_{III} at the end of the stiffener flange are calculated by combining the G_0-values per unit load and the element forces using G-value superposition. The G_I, G_{II} and G_{III} at the end of the stiffener flange were calculated as

$$G_I = (M\sqrt{G_{IM0}} - T\sqrt{G_{IT0}} + F\sqrt{G_{IF0}})^2 \qquad (2)$$

$$G_{II} = (M\sqrt{G_{IIM0}} + T\sqrt{G_{IIT0}} + F\sqrt{G_{IIF0}})^2 \qquad (3)$$

$$G_{III} = (S\sqrt{G_{IIIS0}})^2, \qquad (4)$$

where

M : bending moment per unit width at the end of the stiffener flange,

T : tension load per unit width at the end of the stiffener flange,

F : out-of-plane shear load per unit width at the end of the stiffener flange,

S : in-plane shear load per unit width at the end of the stiffener flange,

G_0 : G-value computed per unit load at the end of the stiffener flange.

3.3 Prediction of failure strength

The proposed method of predicting the failure strength is verified using the buckling test results of the stiffened panels in reference [3]. The configurations of the stiffened panels are shown in Fig. 7. The test material was Toho Tenax UT500/#135. The skins and stiffeners were cocured with no adhesive. A picture frame fixture was used to introduce pure shear load to a test panel for the shear panel test in Fig. 8(a). The end of the compression panel was inserted in the aluminum end fixture with epoxy resin in Fig. 8(b).

3.3.1 Postbuckling analysis

To compute the element forces at the end of the stiffener flange, the stiffened panel was postbuckling-analyzed. The element forces are the tension load T, bending moment M, out-of-plane shear load F, and in-plane shear load S on the element of the skin under the end of the stiffener flange.

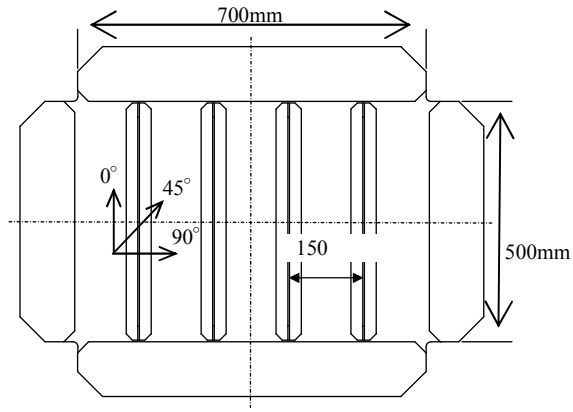

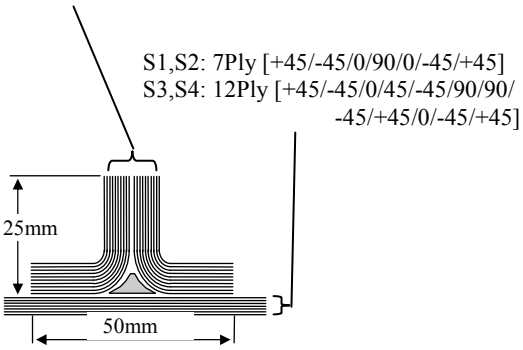

(a) Shear panel

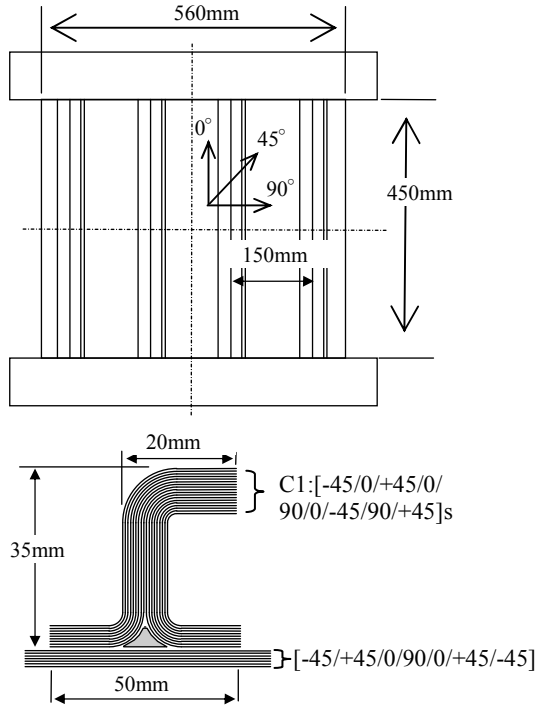

(b) Compression panel

Fig. 7. Stiffened panel configurations [3].

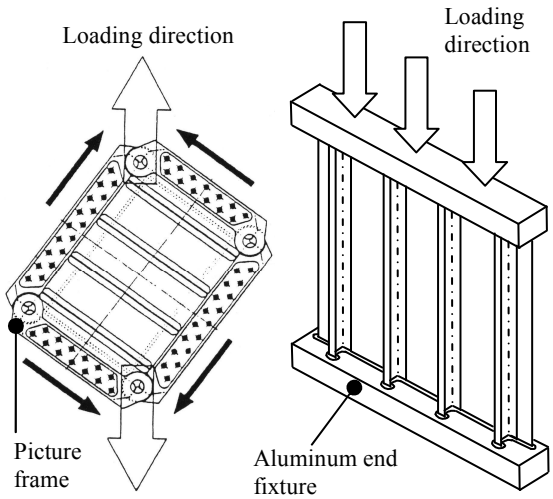

(a) Shear test (b) Compression test

Fig. 8. Buckling test setup.

FEM analysis was carried out using in the ABAQUS finite element system. The shear and compression panels were modeled using eight-node shell elements. Figure 9 shows the FEM model. The aluminum end fixture of the compression panel was modeled using eight-node solid elements. Figure 10 shows the FEM model of the end of the stiffener flange. The forces on the element of the skin at the end of the stiffener flange (part A in the figure) were extrapolated from the element forces at B and C. The initial imperfection was used from the results of linear buckling eigenvalue analysis.

Linear buckling eigenvalue analysis results are given in Table 4. Figure 11 shows the out-of-plane deformation of the stiffened panel computed under shear loading and compression loading. The deformation mode corresponds with the moiré interferometry measurement results. Figure 12 shows the out-of-plane displacement at the center line of the panel. The correlation of postbuckling analysis results and experimental results is good.

3.3.2 Calculating energy release rate

Figure 13 shows G-values distribution along the end of the stiffener flange in the shear panel S1. Substitution of the element forces mentioned earlier in equations (2) to (4) leads to the G-values at the end of the stiffener flange by the applied load. The G-value of the vertical axis in the figure is shown as the normalized value with respect to G_C of each mode. G_I and G_{II} have three peaks. The peak locations agreed. On the other hand, the three peak locations of G_{III} are shifted from the peak locations of G_I and G_{II}. G_{III} increases as the applied load

increases at all locations.

Figure 14 shows G-values distribution along the end of the stiffener flange in the compression panel C1. The G-value of the vertical axis in the figure is shown as the normalized value with respect to G_C of each mode. G_I has three peaks. The three peak locations of G_{II} change as the applied load increases. The peak locations of G_{III} are at the top and bottom ends in the stiffened panel.

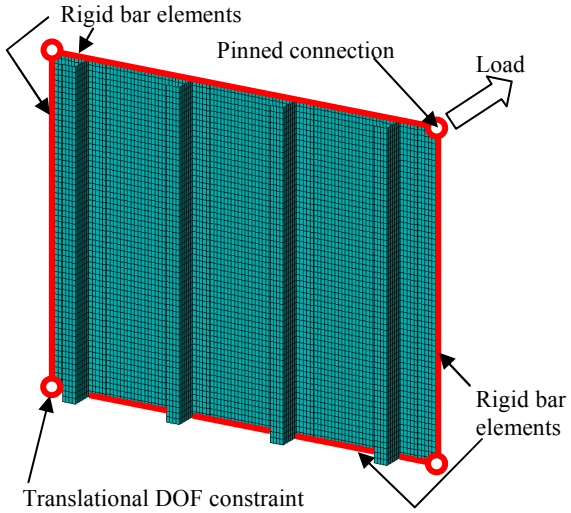

(a) Shear panel

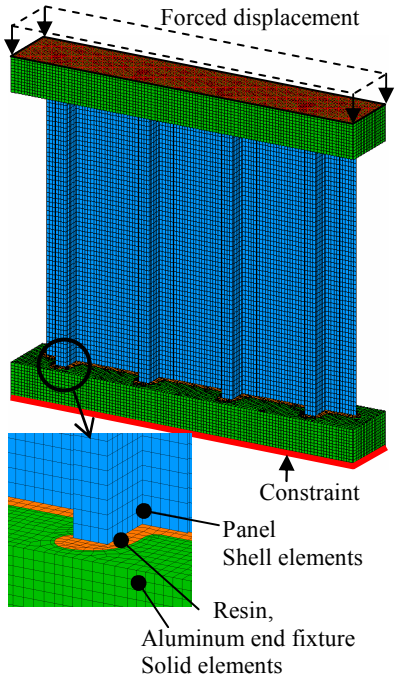

(b) Compression panel

Fig. 9. FEM models of stiffened panels.

Figure 15(a) shows the relationship between the G-value of each mode and the applied load at -132 mm in the Z direction of the stiffener flange in the shear panel S1. Figure 15(b) shows the relationship between the G-value of each mode and the applied load at -206 mm in the Z direction of the stiffener flange in the compression panel C1. At both locations, G_I is equivalent to 0. In Fig. 15, G_I is not shown. In both cases, G_{III}/G_{IIIC} increases as the applied load increases. G_{III} affects the failure load for S1 and C1, in contrast to G_I and G_{II}.

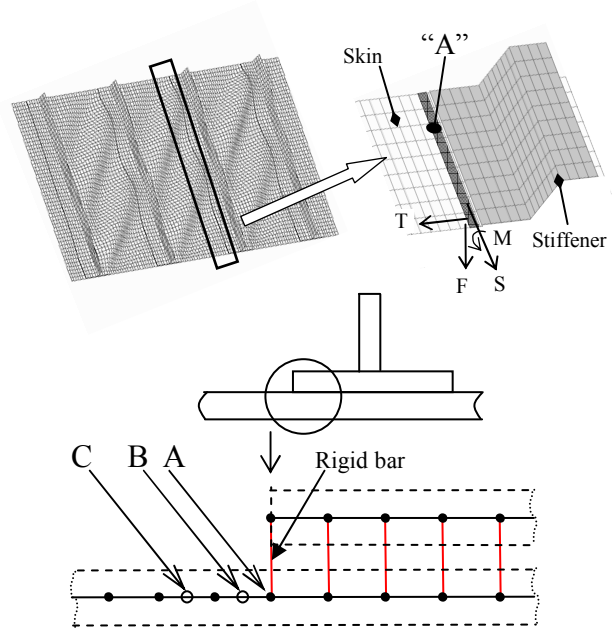

Fig. 10. FEM shell model for postbuckling analysis .

Table 4. FEM results of buckling load [3].

Test	Panel No.	Buckling load (kN)	
		Experiment	FEM
Shear	S1	42.5	37.7
	S2	45.4	
	S3	179	133.4
	S4	199	162.5
Compression	C1	57.2	71.9

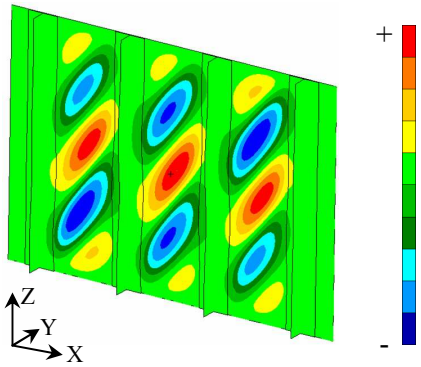

(a) Shear test, S1

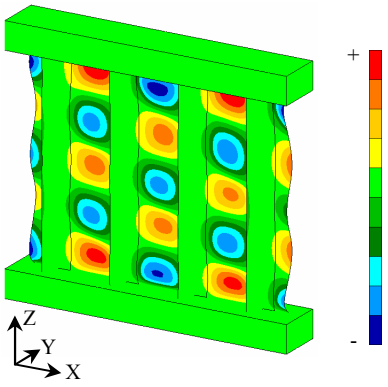

(b) Compression test, C1

Fig. 11. Buckling deformation of stiffened panels.

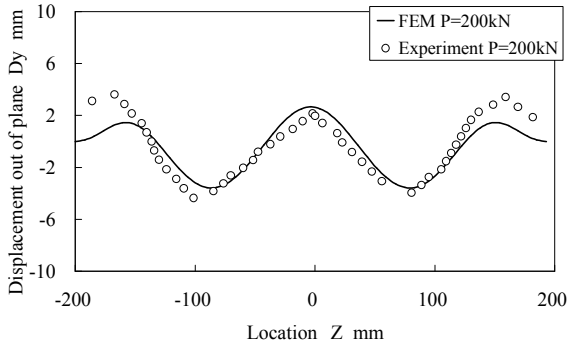

(a) Shear test, S1

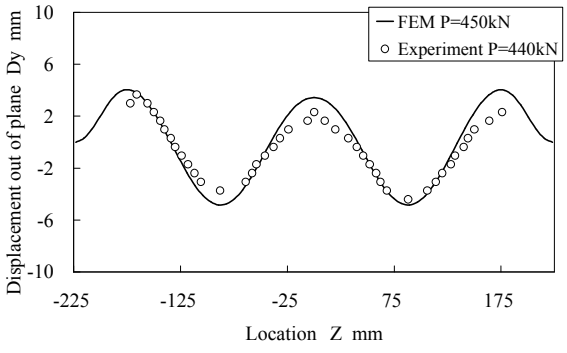

(b) Compression test, C1

Fig. 12. Deformation at the center line of the panel.

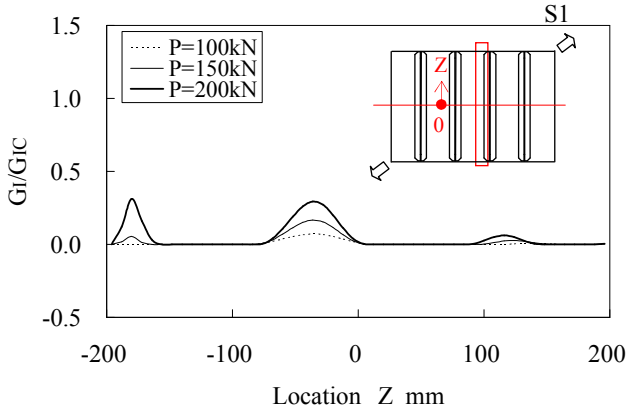

(a) G_I

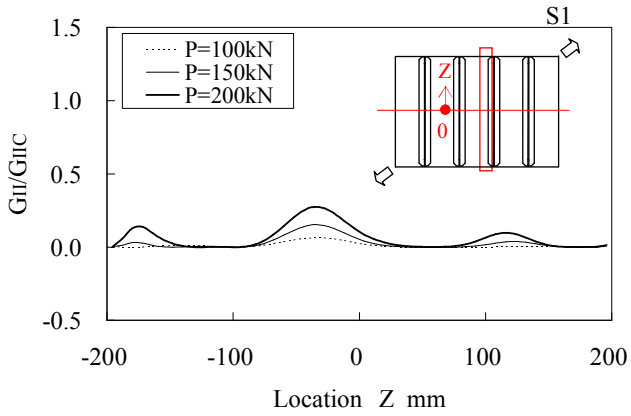

(b) G_{II}

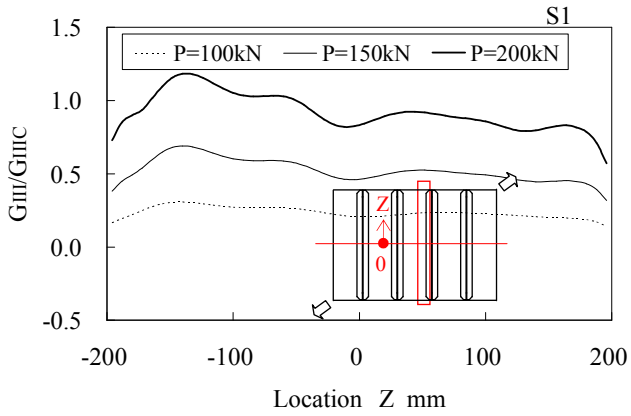

(c) G_{III}

Fig. 13. G-values distribution along the end of the stiffener flange in shear panel S1.

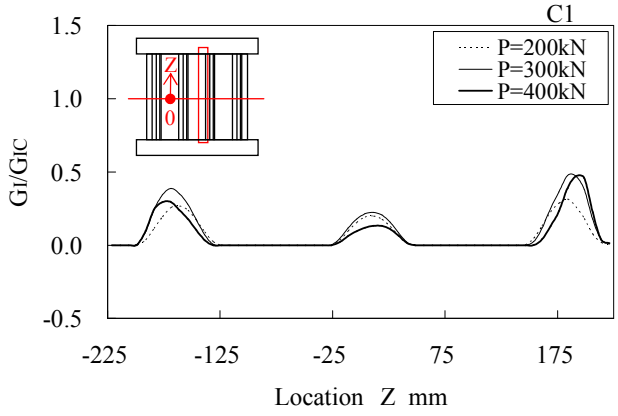

(a) G_I

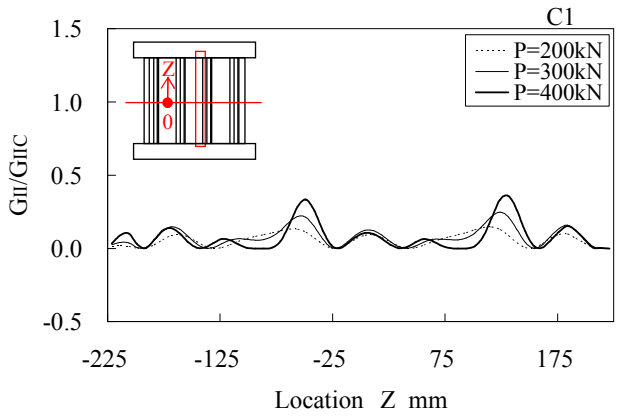

(b) G_{II}

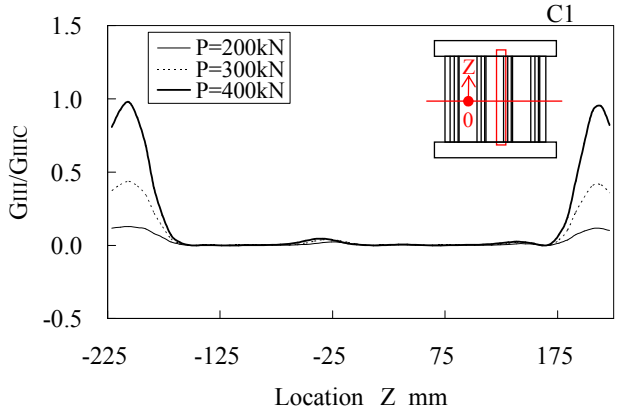

(c) G_{III}

Fig. 14. G-values distribution along the end of the stiffener flange in compression panel C1.

3.3.3 Fracture load estimation

Figure 16 shows the failure criterion for the load applied to the stiffened panel. Substitution of the G-values at the end of the stiffener flange in equation (1) leads to the failure criterion. When the

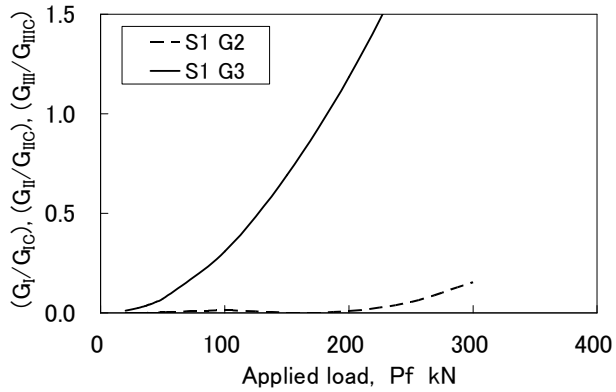

(a) Shear test, S1

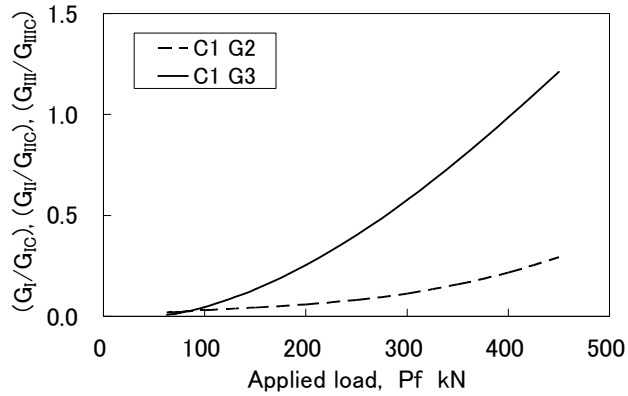

(b) Compression test, C1

Fig. 15. Relation between G-values and applied load.

failure criterion is 1, the load applied to the stiffened panel is taken to be the predicted failure load.

Figure 17 shows the comparison between measured failure load and predicted failure load. The predicted failure load agreed well with the measured failure load.

4 Conclusion

A method of predicting the failure strength after buckling in composite stiffened panels was proposed. The failure loads of the compression and shear buckling tests in reference [3] were predicted. This method showed a good correlation between predicted failure load and measured failure load.

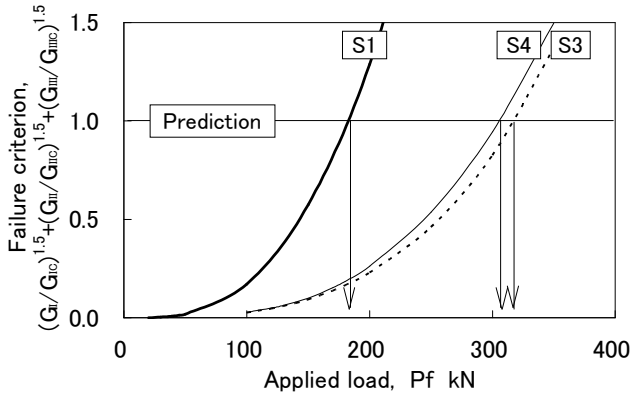

(a) Shear test, S1

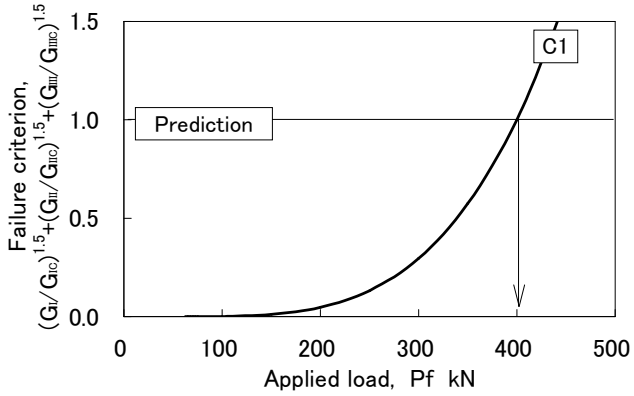

(b) Compression test, C1

Fig. 16. Failure criterion value for the applied load

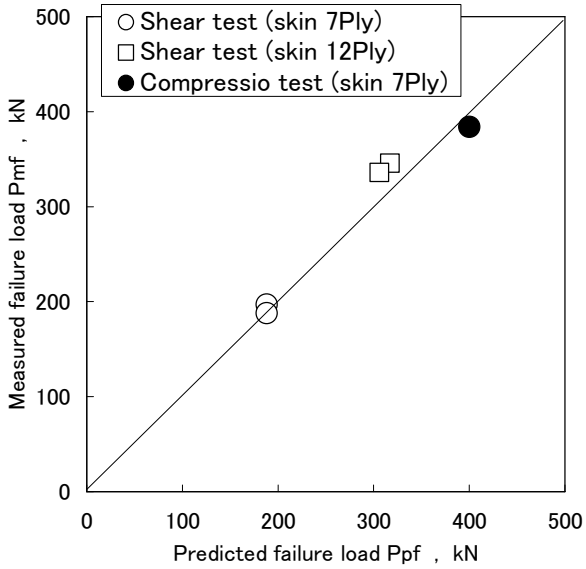

Fig. 17. Comparison between measured failure load [3] and predicted failure load.

References

[1] Wang J.T., Raju I.S, and Sleight D.W. "*Composite Skin-stiffener Debond Analyses Using Fracture Mechanics Approach with Shell Elements*". Composite Eng, Vol. 5, No. 3, pp 277-296, 1995.

[2] Minguet P.J. and O'Brien T.K. "*Analysis of test methods for characterizing skin/stringer debonding failures in reinforced composite panels*". ASTM STP 1274, pp 105-124, 1996.

[3] JADC "*Composite Material Strength Evaluation DATA BASE*". 1998.